

## HYDRODYNAMIC STABILITY CLOSE TO A ROTATING DISK ELECTRODE WITH RESPECT TO AXISYMMETRIC PERTURBATIONS

JOSÉ PONTES\*, NORBERTO MANGIACACCHI†, OSWALDO E. BARCIA‡, OSCAR R. MATTOS§,  
BERNARD TRIBOLLET¶, AND DANIEL WALGRAEF||

**Abstract.** Polarization curves experimentally obtained in the electro-dissolution of iron in a 1 M  $\text{H}_2\text{SO}_4$  solution using a rotating disk as the working electrode present a current instability region within the range of applied voltage in which the current is controlled by mass transport in the electrolyte. According to the literature (Barcia et. al., 1992) the electrodissolution process leads to the existence of a viscosity gradient in the interface metal-solution, which changes the velocity profiles and may affect the stability of the hydrodynamical field. The purpose of this work is to investigate whether this viscosity gradient may lead to a hydrodynamic instability. Two classes of perturbations are considered: perturbations monotonically varying along the radial direction and perturbations periodically modulated along the radial direction. The results show that the hydrodynamic field is always stable with respect to the first class of perturbations but that the neutral stability curves are significantly modified by the presence of a viscosity gradient in the second case. The critical Reynolds number, above which the considered class of perturbations are linearly unstable, is clearly reduced. The existence of unstable hydrodynamic modes at Reynolds numbers on the order of those found in the experimental setup may originate the observed current instability.

**1. Introduction.** Polarization curves experimentally obtained in the electro-dissolution of iron in a 1 M  $\text{H}_2\text{SO}_4$  solution using a rotating disk as the working electrode present three different regions (Barcia et. al., 1992). In the first region, associated with low overvoltages applied to the working electrode, the current is a function of the electric potential and dissolution process only. The electric current is controlled by the transfer of charges at the interface rotating disk/electrolyte solution, and the mass transport does not affect the electro-dissolution process. By increasing the applied potential, the curves show a second region where the hydrodynamic conditions, which depend on the angular velocity imposed to the rotating disk electrode, affect the rate of the anodic dissolution of iron. The current is a function both of the applied potential and the hydrodynamic field developed close to the rotating electrode. By further increasing the applied overvoltage, a third region appears, where the current is totally controlled by mass-transport processes. In this third region, polarization curves present a current plateau, defining a limit value for the current, which depends on the hydrodynamic conditions set by the angular velocity of the electrode.

Two current instabilities are observed in the third region, one at the beginning of the current plateau and the second one at the end, where the electrode surface undergoes an active to passive transition (Ferreira et. al., 1994). The first instability is intrinsic to the system, while the current instability close to the active/passive transition is affected by the output impedance of the control equipment. This instability can be suppressed by using a negative feedback resistance (Epelboim, 1972), that gives rise to a continuous curves.

Most explanations presented in the literature for the current instabilities are based on mechanisms proposing on a  $\text{FeSO}_4$  film precipitated at the electrode surface (Russel and Newman, 1986). In fact, changes in the ohmic voltage drop due to precipitation and dissolution of a  $\text{FeSO}_4$  film provide an acceptable explanation for the instability observed in the active/passive transition region, coupled with the output impedance of the control equipment. However, this model can not be

\* Metallurgy and Materials Engineering Department – EE/COPPE/UFRJ, PO Box 68505, 21945-970 Rio de Janeiro RJ, Brazil [jopontes@ufrj.br](mailto:jopontes@ufrj.br)

† Institute of Mathematical and Computational Sciences USP – S. Carlos, PO Box 668, 13560-161 S.Carlos, SP, Brazil [norberto@icmc.sc.usp.br](mailto:norberto@icmc.sc.usp.br)

‡ Institute of Chemistry – UFRJ, 21945-970 Rio de Janeiro, Brazil [barcia@metalmat.ufrj.br](mailto:barcia@metalmat.ufrj.br)

§ Metallurgy and Materials Engineering Department – COPPE/UFRJ, PO Box 68505 21945-970 Rio de Janeiro RJ, Brazil [omattos@metalmat.ufrj.br](mailto:omattos@metalmat.ufrj.br)

¶ UPR15 – CNRS, Physique des Liquides et Electrochimie, 4 place Jussieu, 75252 Paris Cedex 05, France

|| Center for Nonlinear Phenomena and Complex Systems, Université Libre de Bruxelles CP 231, B-1050 Brussels, Belgium [dwaegr@ulb.ac.be](mailto:dwaegr@ulb.ac.be)

generalized to explain oscillations observed at the begining of the current plateau. By using electro-hydrodynamic (EHD) impedance measurements, Barcia et. al. (1992) studied the electro-dissolution of iron electrodes in 1 M H<sub>2</sub>SO<sub>4</sub> at the current plateau before and after the first instability region. EHD impedance is a non-stationary method which introduces a perturbation with variable frequency and low amplitude in the angular velocity of the rotating disk electrode (Tribollet and Newman, 1983). The perturbation in the angular velocity of the electrode induces a perturbation in the hydrodynamic and mass boundary layers which affects the mass transport and, consequently, the current response at constant applied overvoltage. Analysis of the EHD impedance results provides information on the state of the electrode surface. In particular it gives information on whether the surface is partially blocked (Caprani, 1987), uniformly accessible or covered by a porous film (Deslouis, 1987). Barcia et. al. (1992) verified that the electrode surface is uniformly accessible before and after the first current instability, showing that the surface is not covered by a film. In these conditions it is highly improbable that the electro-dissolution kinetics leads to the deposition of a film in the begining of the first instability region and that this film disappears at the end of that region, in order to restore the steady-state current at the same level observed before the onset of the instability. Moreover, Barcia et. al. (1992) propose that the electro-dissolution process leads to the existence of a viscosity gradient in the diffusion boundary layer. This viscosity gradient could affect the stability of the hydrodynamic field and explain the observed current instability.

On the other hand, the existence of an hydrodynamic instability in the boundary layer which develops close to a rotating disk has been the object of a number of investigations, both experimental and theoretical in the case of fluids with uniform viscosity. For a comprehensive review of the literature on the subject the reader is referred to the paper of Reed and Saric (1989). The main result concerning the stability of the steady state velocity field is that the flow becomes unstable beyond a certain distance from the axis of rotation. The flow develops corotating vortices which spiral outward with their axes along logarithmic spirals of angle 90° + ε (ε ≈ 13°) with respect to radius of the disk. The first study of transition on a rotating disk, due to Smith (1946), found sinusoidal disturbances in the boundary layer. Subsequently, Gregory, Stuart & Walker (1955) found stationary vortices from a nondimensional radius  $R = 430$  in a flow visualization using the wet-china-clay technique. Here the nondimensional radius  $R$ , or *Reynolds number*, is defined by

$$(1.1) \quad R = r \left( \frac{\Omega}{\nu(\infty)} \right)^{1/2}$$

where  $r$  is the radial distance from the axis,  $\Omega$  and  $\nu(\infty)$  are the angular velocity and the viscosity far from the disk surface. The experimental critical value of  $R$  found in the literature, below which all small disturbances dampen, has been reported as being anywhere between 182 and 530. As pointed out by Wilkinson & Malik (1985), “the discrepancy between the values of critical Reynolds number obtained from hot-wire studies and the earlier relatively high values obtained by visual techniques clearly results from the insensitivity of visual techniques to very small disturbances”.

Among the numerous analytical works, the work of Malik (1986) is of particular relevance. This author determined the neutral stability curve (in the plane  $R \times \kappa$ ) for stationary vortex disturbances using a system of linear stability equations which include the effects of streamline curvature and Coriolis force. Here  $\kappa$  is the nondimensional perturbation wavenumber, defined by

$$(1.2) \quad \kappa = \frac{2\pi}{\lambda_d \left( \frac{\Omega}{\nu(\infty)} \right)^{1/2}}$$

where  $\lambda_d$  is the dimensional wavelength of the perturbation. The critical Reynolds number was found to be in good agreement with experimental results, at a value of  $R = 285.36$ .

We emphasize that all these results refer to constant viscosity fluids. If we consider these results alone we cannot explain the observed instability in the electrochemical cell since Reynolds numbers in these experiments are always less than 100, and no experimental study reports instability below  $R=182$  for the case of constant viscosity.

To investigate the importance of the hydrodynamics in the electro-dissolution of iron, Ferreira (1993) and Geraldo (1998) studied the influence of the viscosity on the current oscillations observed at the begining of the current plateau region measured in electrochemical cells where the working electrode consists of a rotating disk. These authors found that increasing the electrolyte viscosity – and therefore decreasing the Reynolds number – by adding glycerol to the solution, forces the current oscillations to a periodic behaviour or even suppresses the instability. The facts that no hydrodynamic instability is observed in the range of Reynolds numbers of the experiments for the case of constant viscosity, and that a viscosity gradient has been observed in the boundary layer in the electrochemical cells, suggest that the viscosity gradient may play an important role in the hydrodynamic stability of the flow and may therefore affect the electric current.

The purpose of this work is to investigate the influence of a viscosity gradient along the axial direction, on the stability of the boundary layer developed close to the rotating disk electrode with respect to two classes of axisymmetric perturbations. The first class consists of perturbations with a structure quite close to the structure of the base state, with no periodic variations along the radial direction. In the second class, a periodic variation along  $r$  is assumed.

A small perturbation is added to the steady-state hydrodynamic field and the evolution of the perturbed field is investigated with the appropriate linearized form of the evolution equations. Space derivatives are discretized transforming the original formulation in a generalized eigenvalue/eigenvector problem. The eigenvectors contain a description of each perturbation mode in the points of the grid. The sign of the real part of the associated eigenvalue defines the stability of the mode and the imaginary part determines the natural frequency of the mode. The problem is solved numerically.

Section 2 presents the evolution equations governing the hydrodynamic field, the form of the viscosity profile assumed and the steady-state solution of the problem for both constant and variable viscosity fluids. Sections 3 and 4 present the linear stability analysis of the hydrodynamic field with respect to the first and the second class of perturbations considered and Section 5 presents the conclusions of this work.

**2. The Steady-State Hydrodynamic Field.** In this section we describe the steady-state solution of the continuity and time-dependent Navier-Stokes equations for infinite rotating disk (Schlichting, 1968) and variable viscosity fluids, given by Eqs. (2.1-2.4).

$$(2.1) \quad \frac{\partial v_r}{\partial r} + \frac{v_r}{r} + \frac{\partial v_z}{\partial z} = 0$$

$$(2.2) \quad \frac{\partial v_r}{\partial t} + v_r \frac{\partial v_r}{\partial r} - \frac{v_\theta^2}{r} + v_z \frac{\partial v_r}{\partial z} = -\frac{1}{\rho} \frac{\partial p}{\partial r} + \nu \left( \frac{\partial}{\partial r} \left( \frac{1}{r} \frac{\partial}{\partial r} r v_r \right) + \frac{\partial^2 v_r}{\partial z^2} \right) + \frac{\partial \nu}{\partial z} \left( \frac{\partial v_z}{\partial r} + \frac{\partial v_r}{\partial z} \right)$$

$$(2.3) \quad \frac{\partial v_\theta}{\partial t} + v_r \frac{\partial v_\theta}{\partial r} + \frac{v_r v_\theta}{r} + v_z \frac{\partial v_\theta}{\partial z} = \nu \left( \frac{\partial}{\partial r} \left( \frac{1}{r} \frac{\partial}{\partial r} r v_\theta \right) + \frac{\partial^2 v_\theta}{\partial z^2} \right) + \frac{\partial \nu}{\partial z} \frac{\partial v_\theta}{\partial z}$$

$$(2.4) \quad \frac{\partial v_z}{\partial t} + v_r \frac{\partial v_z}{\partial r} + v_z \frac{\partial v_z}{\partial z} = -\frac{1}{\rho} \frac{\partial p}{\partial z} + \nu \left( \frac{1}{r} \frac{\partial}{\partial r} \left( r \frac{\partial v_z}{\partial r} \right) + \frac{\partial^2 v_z}{\partial z^2} \right) + 2 \frac{\partial \nu}{\partial z} \frac{\partial v_z}{\partial z}$$

The steady-state hydrodynamic field for constant-viscosity fluids close to the axis of a rotating disk was first investigated by von Kármán (1921). As a necessary prelude to the following sections we briefly review von Kármán results (Schlichting, 1968).

Introducing in Eqs. (2.2-2.4) the dimensionless functions  $F$ ,  $G$ ,  $H$  and  $P$ , defined by:

$$(2.5) \quad \bar{v}_r = r \Omega F(\xi)$$

$$(2.6) \quad \bar{v}_\theta = r \Omega G(\xi)$$

$$(2.7) \quad \bar{v}_z = (\nu(\infty) \Omega)^{1/2} H(\xi)$$

$$(2.8) \quad \bar{p} = \rho \nu(\infty) \Omega P(\xi)$$

where  $\xi = z(\Omega/\nu(\infty))^{1/2}$  and  $\Omega$  is the angular velocity of the disk, we obtain a set of three coupled nonlinear ordinary differential equations for the dimensionless functions  $F$ ,  $G$  and  $H$  and a fourth equation for  $P$ .

In the case of electrolytes with variable viscosity we consider that the transport properties depend on  $\xi$  only. Consequently von Kármán's transformations (von Karmán, 1921) given by Eqs. (2.5-2.8) can be used. The problem for variable density and viscosity fluids was studied by Pollard and Newman (1980). In the present case the density is assumed to be constant. By introducing the dimensionless functions in Eqs. (2.2-2.4) we obtain:

$$(2.9) \quad 2F + H' = 0$$

$$(2.10) \quad F^2 - G^2 + HF' = \frac{\partial}{\partial \xi} \left( \frac{\nu(\xi)}{\nu(\infty)} F' \right)$$

$$(2.11) \quad 2FG + HG' = \frac{\partial}{\partial \xi} \left( \frac{\nu(\xi)}{\nu(\infty)} G' \right)$$

$$(2.12) \quad P' + HH' = 2 \frac{\nu'(\xi)}{\nu(\infty)} H' + \frac{\nu(\xi)}{\nu(\infty)} H''$$

Boundary conditions for  $F$ ,  $G$  and  $H$  are  $F = H = P = 0$ ,  $G = 1$  when  $\xi = 0$ ,  $F = G = H' = 0$  when  $\xi \rightarrow \infty$ . Conditions  $F = 0$  and  $G = 1$  in  $\xi = 0$  reflect the non-slip requirement at the electrode surface. To integrate the above equations it is necessary to impose a viscosity profile. In this work we use the following profile proposed by Barcia et. al. (1992):

$$(2.13) \quad \frac{\nu(\xi)}{\nu(\infty)} = \frac{\nu(0)}{\nu(\infty)} + \left( 1 - \frac{\nu(0)}{\nu(\infty)} \right) \frac{q^{1/3}}{\Gamma(4/3)} \int_0^\xi e^{-q\xi^3} d\xi$$

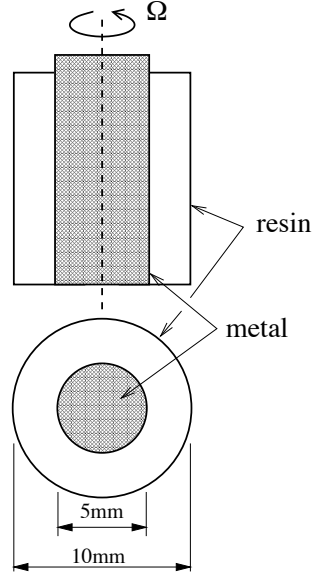


Fig. 1: The rotating disk electrode

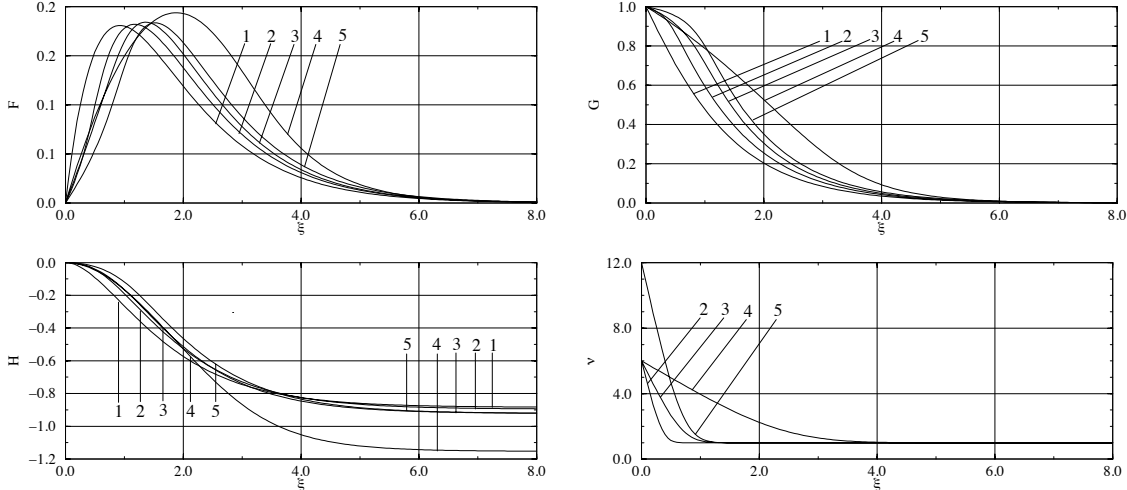


Fig. 2: Dimensionless velocity profiles  $F$ ,  $G$  and  $H$  and viscosity profiles. Curves No. 1 refer to constant viscosity fluid. Curves Nos. 2 – 5 refer to variable viscosity fluids with the following parameters: Curves No. 2:  $\nu(0)/\nu(\infty) = 6$  and  $q = 15$ ; Curves No. 3:  $\nu(0)/\nu(\infty) = 6$  and  $q = 2$ ; Curves No. 4:  $\nu(0)/\nu(\infty) = 6$  and  $q = 0.05$ ; Curves No. 5:  $\nu(0)/\nu(\infty) = 12$  and  $q = 2$ .

The term  $\nu(0)/\nu(\infty)$  in Eq. (2.13) is the ratio of the viscosity at the electrode surface and in the bulk of solution. Although the calculation is, strictly speaking, applicable to an infinite disk only, we utilize the same results when working experimentally with a finite disk, provided that the disk radius is large compared with the thickness of the layer carried with the disk. Fig. 1 shows a rotating disk used in electrochemistry. This electrode consists of a cylindrical rod ( $A=0.2 \text{ cm}^2$ ). The rod specimen is embedded in an epoxy resin mold such that only its cross section is allowed to contact the electrolyte, in order to constitute a rotating disk electrode. Figure 2 shows the velocity and viscosity profiles used in this work.

**3. Stability With Respect to Perturbations Monotonically Varying Along the Radial Direction.** We now address the problem of the stability of the base state with respect to small perturbations in the form:

$$(3.1) \quad \tilde{v}_r = e^{\lambda t} r \Omega f(\xi)$$

$$(3.2) \quad \tilde{v}_\theta = e^{\lambda t} r \Omega g(\xi)$$

$$(3.3) \quad \tilde{v}_z = e^{\lambda t} (\nu(\infty) \Omega)^{1/2} h(\xi)$$

where  $\lambda$  is a parameter to be determined. We look for a solution of Eqs. (2.1-2.3) in the form of base state plus above perturbations. Since small perturbations are considered, non-linear terms may be neglected leading to the following linearized evolution equations for the perturbations:

$$(3.4) \quad \left( \frac{1}{r} + \frac{\partial}{\partial r} \right) \tilde{v}_r + \frac{\partial \tilde{v}_z}{\partial z} = 0$$

$$(3.5) \quad \frac{\partial \tilde{v}_r}{\partial t} + \bar{v}_r \frac{\partial \tilde{v}_r}{\partial r} + \tilde{v}_r \frac{\partial \bar{v}_r}{\partial r} - \frac{2\bar{v}_\theta \tilde{v}_\theta}{r} + \bar{v}_z \frac{\partial \tilde{v}_r}{\partial z} + \tilde{v}_z \frac{\partial \bar{v}_r}{\partial z} = \nu \frac{\partial^2 \tilde{v}_r}{\partial z^2} + \frac{\partial \nu}{\partial z} \frac{\partial \tilde{v}_r}{\partial z}$$

$$(3.6) \quad \frac{\partial \tilde{v}_\theta}{\partial t} + \bar{v}_r \frac{\partial \tilde{v}_\theta}{\partial r} + \tilde{v}_r \frac{\partial \bar{v}_\theta}{\partial r} + \frac{\bar{v}_r \tilde{v}_\theta + \tilde{v}_r \bar{v}_\theta}{r} + \bar{v}_z \frac{\partial \tilde{v}_\theta}{\partial z} + \tilde{v}_z \frac{\partial \bar{v}_\theta}{\partial z} = \nu \frac{\partial^2 \tilde{v}_\theta}{\partial z^2} + \frac{\partial \nu}{\partial z} \frac{\partial \tilde{v}_\theta}{\partial z}$$

The expressions of the base state and of the perturbations are now inserted in the linearized evolution equations. By defining the non-dimensional viscosity as  $\nu^* = \nu(\xi)/\nu(\infty)$  and dropping the asterisk from the new variable we obtain:

$$(3.7) \quad 2f + h' = 0$$

$$(3.8) \quad \nu f'' + \nu' f' - H f' - 2F f + 2G g - F' h = \frac{\lambda}{\Omega} f$$

$$(3.9) \quad -2G f + \nu g'' + \nu' g' - H g' - 2F g - G' h = \frac{\lambda}{\Omega} g$$

Variables  $f$ ,  $f'$  and  $f''$  may be eliminated by replacing:

$$f = -\frac{h'}{2} \quad f' = -\frac{h''}{2} \quad f'' = -\frac{h'''}{2}$$

We arrive at a two-equations system, one containing third-order space derivatives and the other one with second-order space derivatives. The system reads:

$$(3.10) \quad \begin{pmatrix} \nu D^3 + (\nu' - H) D^2 - 2FD + 2F'; -4G \\ GD - C'; \nu D^2 + (\nu' - H) D - 2F \end{pmatrix} \begin{pmatrix} h \\ g \end{pmatrix} = \frac{\lambda}{\Omega} \begin{pmatrix} D & 0 \\ 0 & 1 \end{pmatrix} \begin{pmatrix} h \\ g \end{pmatrix}$$

where  $D^n = d^n/d\xi^n$ . Eq. (3.10) defines a generalized eigenvalue/eigenfunction problem. The eigenfunctions are the normal modes of the model, the real and the imaginary parts of each eigenvalue being the rate of growth and frequency of the associated mode.

The sole parameters appearing in this eigenvalue/eigenfunction problem are those associated with the viscosity profile,  $\nu(0)/\nu(\infty)$  ratio and  $q$  (see Eq. 2.13) which define the slope of the profile close to the electrode surface.

Boundary conditions of the problem require non-slip flow and vanishing axial component of the velocity at the electrode surface. These conditions are already fulfilled by the base-state, so the hydrodynamic field cannot be modified by the perturbation at the electrode surface. In consequence we must require  $g = h = 0$  in  $\xi = 0$ . Moreover, we conclude from Eq. (4.4) that  $h' = 0$  at the electrode surface. In  $\xi \rightarrow \infty$  we require that the perturbation vanishes ( $g = h = 0$ ) and that  $g' = 0$ .

The generalized eigenvalue/eigenfunction problem is solved numerically. Space derivatives are represented by the following second-order discrete formulæ, transforming the original problem in an

eigenvalue/eigenvector problem.

$$\begin{aligned} X_{i+1/2} &= \frac{1}{2}(X_i + X_{i+1}) \\ X'_{i+1/2} &= \frac{1}{\Delta\xi}(-X_i + X_{i+1}) \\ X''_{i+1/2} &= \frac{0.5}{\Delta\xi^2}(X_{i-1} - X_i - X_{i+1} + X_{i+2}) \\ X'''_{i+1/2} &= \frac{1}{\Delta\xi^3}(-X_{i-1} + 3X_i - 3X_{i+1} + X_{i+2}) \end{aligned}$$

The problem is solved using the LAPACK double precision *dgeev* routine for real generalized nonsymmetric eigenproblems.

**3.1. Results.** The results of the linear stability analysis are shown in Figs. (3) and (4).

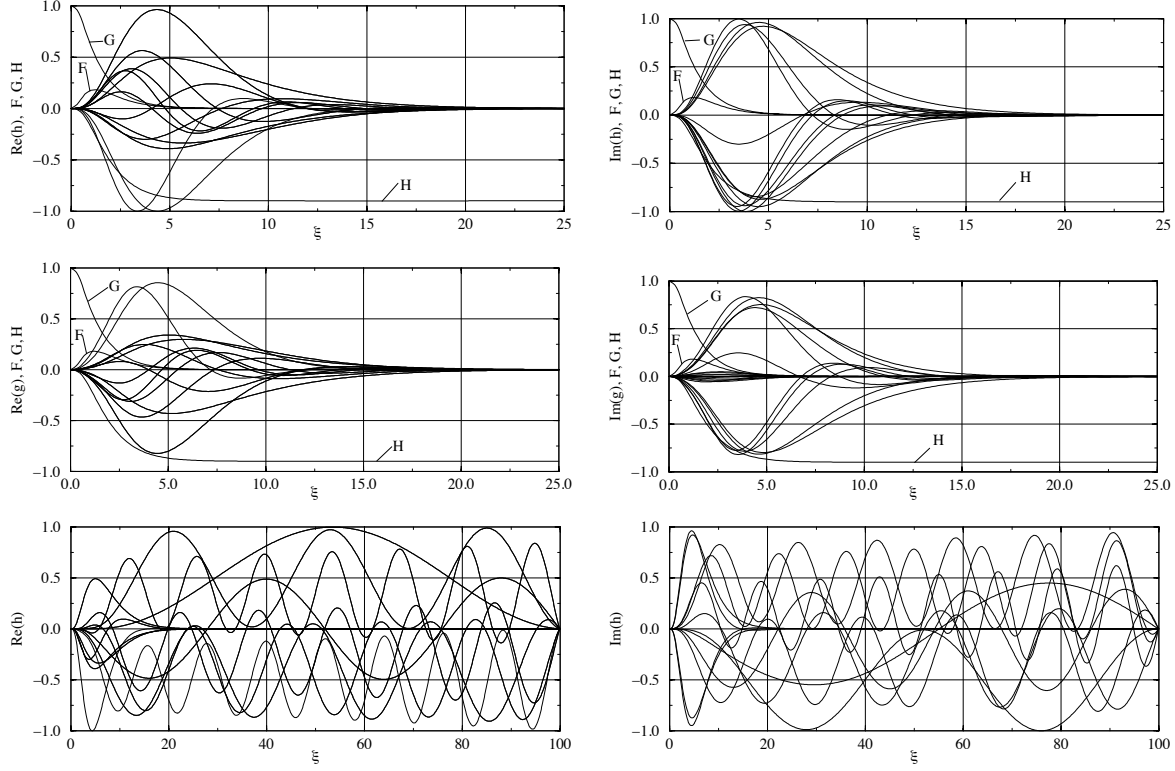


*Fig. 3: On top: real and imaginary parts of boundary layer perturbation modes of  $h$ . Second line: real and imaginary parts of boundary layer perturbation modes of  $g$ . Third line: real and imaginary parts of full layer modes of  $h$ .*

Figure (3) shows the eigenfunctions obtained for the variable viscosity case, along with the associated dimensionless base state velocity profiles  $F$ ,  $G$  and  $H$ . Only eigenfunctions of the variable viscosity case are shown since modes of the constant viscosity case are qualitatively similar to the former ones. These figures show that the model described by contains *two* classes of modes:

- Boundary layer modes;
- Full-length modes.

Boundary layer modes are those that decay after a certain distance from the electrode surface. They exist due to the form of the steady state hydrodynamic boundary layer developed close to the electrode surface. Nevertheless, these modes are longer than the steady state profiles,

in the sense that the distance from the electrode surface at which the former assume the asymptotic value is at least two times the distance required by the latter to assume that value. In most cases boundary layer modes present a spatial oscillation along the axial direction, and do have a non-vanishing mean value. If we consider the axial component of velocity, this result indicates that the perturbation disturbs the vertical flow rate of the electrolyte and, by continuity, the flow in the radial direction. Mass transport is thus affected by this class of perturbations.

Full-length modes are those that do not decay far from the electrode surface. Figure (3) shows the fundamental and the first higher order full-length modes. These modes also have a non-vanishing mean value, thus affecting the electrolyte flow rate in the axial and radial directions.

Full-length modes are observed in perturbations of the axial velocity component only. This difference can be explained by the fact that boundary conditions applicable to the axial component of the velocity at the system end opposite to the electrode surface are looser than those applicable to the  $g$  profile, associated to the tangential component of the velocity.

The eigenvalues obtained for both cases are presented in Fig. (4), in the form of three diagrams containing  $\Re(\omega/\Omega) \times \Im(\omega/\Omega)$ . The diagram shown on top of Fig. (4) contains the full spectra of eigenvalues and the following two show successive zooms of eigenvalues with larger real part.

The real part of the eigenvalues is always *negative*, showing that the system is *stable* to the class of perturbations considered in this section, no matter if the fluid viscosity is constant or depends on the axial coordinate.

The eigenvalues fall in two curves depending on whether they belong to the class of boundary layer or full-length modes. Eigenvalues associated to boundary layer modes fall in the inner close curve showed in the second diagram of Fig. (4). Frequencies range from a fraction of the angular velocity of the rotating disk, to less than ten times that velocity. Eigenvalues associated to full-length modes fall in the outer curve observed in Fig. (4).

**4. Stability With Respect to Perturbations Periodically Modulated Along the Radial Direction.** We now address the problem of the stability of the base state with respect to small perturbations in the form:

$$(4.1) \quad \tilde{v}_r = e^{\lambda t + i\kappa r} (\nu(\infty) \Omega)^{1/2} f(\xi)$$

$$(4.2) \quad \tilde{v}_\theta = e^{\lambda t + i\kappa r} (\nu(\infty) \Omega)^{1/2} g(\xi)$$

$$(4.3) \quad \tilde{v}_z = e^{\lambda t + i\kappa r} (\nu(\infty) \Omega)^{1/2} h(\xi)$$

where  $\kappa$  is the perturbation wavenumber along the radial direction and  $\lambda$  is the sought eigenvalue of the problem. We look for a solution of the hydrodynamic equations in the form of base state plus perturbations. By eliminating the pressure and neglecting non-linear terms we arrive at the

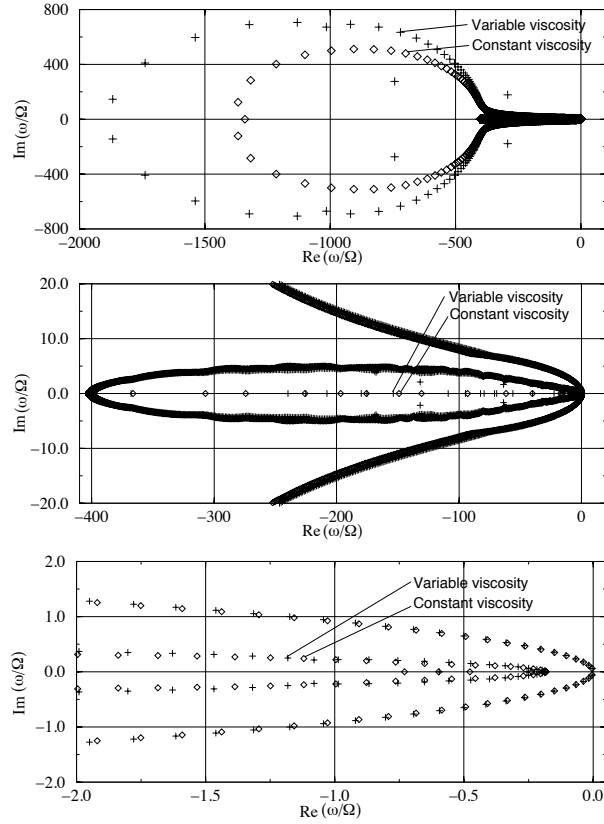


Fig. 4: On top: full spectra of eigenvalues for constant and variable viscosity cases. The following two diagrams show successive zooms of first line, focusing eigenvalues with larger real part

following linearized evolution equations for the perturbations:

$$\begin{aligned}
(4.4) \quad & \left( \frac{1}{r} + \frac{\partial}{\partial r} \right) \tilde{v}_r + \frac{\partial \tilde{v}_z}{\partial z} = 0 \\
& \frac{\partial}{\partial t} \left( \frac{\partial \tilde{v}_r}{\partial z} - \frac{\partial \tilde{v}_z}{\partial r} \right) + \frac{\partial \bar{v}_r}{\partial z} \frac{\partial \tilde{v}_r}{\partial r} + \frac{\partial \tilde{v}_r}{\partial z} \frac{\partial \bar{v}_r}{\partial r} + \bar{v}_r \frac{\partial^2 \tilde{v}_r}{\partial r \partial z} + \tilde{v}_r \frac{\partial^2 \bar{v}_r}{\partial r \partial z} - \frac{2\bar{v}_\theta}{r} \frac{\partial \tilde{v}_\theta}{\partial z} - \frac{2\tilde{v}_\theta}{r} \frac{\partial \bar{v}_\theta}{\partial z} + \\
& \frac{\partial \bar{v}_z}{\partial z} \frac{\partial \tilde{v}_r}{\partial z} + \frac{\partial \tilde{v}_z}{\partial z} \frac{\partial \bar{v}_r}{\partial z} + \bar{v}_z \frac{\partial^2 \tilde{v}_r}{\partial z^2} + \tilde{v}_z \frac{\partial^2 \bar{v}_r}{\partial z^2} - \frac{\partial \bar{v}_r}{\partial r} \frac{\partial \tilde{v}_z}{\partial z} - \bar{v}_r \frac{\partial^2 \tilde{v}_z}{\partial r^2} - \frac{\partial \tilde{v}_z}{\partial r} \frac{\partial \bar{v}_z}{\partial z} - \bar{v}_z \frac{\partial^2 \tilde{v}_z}{\partial r \partial z} = \\
& \frac{d^2 \nu}{dz^2} \left( \frac{\partial \tilde{v}_z}{\partial r} + \frac{\partial \tilde{v}_r}{\partial z} \right) + \frac{d\nu}{dz} \left( -\frac{\tilde{v}_r}{r^2} + \frac{1}{r} \frac{\partial \tilde{v}_r}{\partial r} + \frac{\partial^2 \tilde{v}_r}{\partial r^2} + 2 \frac{\partial^2 \tilde{v}_r}{\partial z^2} - \frac{\partial^2 \tilde{v}_z}{\partial r \partial z} \right) + \\
(4.5) \quad & \nu \left( -\frac{1}{r^2} \frac{\partial \tilde{v}_r}{\partial z} + \frac{1}{r} \frac{\partial^2 \tilde{v}_r}{\partial r \partial z} + \frac{\partial^3 \tilde{v}_r}{\partial z \partial r^2} + \frac{\partial^3 \tilde{v}_r}{\partial z^3} + \frac{1}{r^2} \frac{\partial \tilde{v}_z}{\partial r} - \frac{1}{r} \frac{\partial^2 \tilde{v}_z}{\partial r^2} - \frac{\partial^3 \tilde{v}_z}{\partial r^3} - \frac{\partial^3 \tilde{v}_z}{\partial r \partial z^2} \right) \\
& \frac{\partial \tilde{v}_\theta}{\partial t} + \bar{v}_r \frac{\partial \tilde{v}_\theta}{\partial r} + \tilde{v}_r \frac{\partial \bar{v}_\theta}{\partial r} + \frac{\bar{v}_r \tilde{v}_\theta + \tilde{v}_r \bar{v}_\theta}{r} + \bar{v}_z \frac{\partial \tilde{v}_\theta}{\partial z} + \tilde{v}_z \frac{\partial \bar{v}_\theta}{\partial z} = \\
(4.6) \quad & \nu \left( -\frac{\tilde{v}_\theta}{r^2} + \frac{1}{r} \frac{\partial \tilde{v}_\theta}{\partial r} + \frac{\partial^2 \tilde{v}_\theta}{\partial r^2} + \frac{\partial^2 \tilde{v}_\theta}{\partial z^2} \right) + \frac{d\nu}{dz} \frac{\partial \tilde{v}_\theta}{\partial z}
\end{aligned}$$

We define again the non-dimensional viscosity as  $\nu^* = \nu(\xi)/\nu(\infty)$  and drop the asterisk from the new variable. By inserting the expressions of the base state and of the perturbations in the linearized evolution equations and eliminating the variable  $f$  with the continuity equation we arrive at a two-equation system, one containing fourth-order space derivatives and the other one with second-order space derivatives. The system reads:

$$(4.7) \quad \begin{pmatrix} a_4 D^4 + a_3 D^3 + a_2 D^2 + a_1 D + a_0; & b_1 D + b_0 \\ c_1 D + c_0; & d_2 D^2 + d_1 D + d_0 \end{pmatrix} \begin{pmatrix} h \\ g \end{pmatrix} = \frac{\lambda}{\Omega} \begin{pmatrix} q_2 D^2 + q_0; & 0 \\ 0; & s_0 \end{pmatrix} \begin{pmatrix} h \\ g \end{pmatrix}$$

where  $D^n = d^n/d\xi^n$  and the coefficients in the above operators are given by:

$$\begin{aligned}
a_4 &= \nu & a_3 &= 2\nu' - H \\
a_2 &= -((1+2\kappa^2 R^2)/R^2)\nu + \nu'' - H' - F + i(2\kappa\nu/R - \kappa RF) \\
a_1 &= -((1+2\kappa^2 R^2)/R^2)\nu' + \kappa^2 H + i(2\kappa\nu/R - \kappa H/R) \\
a_0 &= \kappa^2(\nu'' + \kappa^2\nu + 2F + H') + F'' + \\
&\quad i(\kappa RF'' - \kappa(\nu'' + \nu((1+2\kappa^2 R^2)/R^2 + F) + H' - \kappa^2 R^2 F)/R) \\
b_1 &= -2G/R - i(2\kappa G) & b_0 &= -2G'/R - i(2\kappa G') \\
c_1 &= 2RG/(1+\kappa^2 R^2) - i(2\kappa R^2 G/(1+\kappa^2 R^2)) & c_0 &= -RG' \\
d_2 &= \nu & d_1 &= \nu' - H & d_0 &= -((1+\kappa^2 R^2)/R^2)\nu - F + i(\kappa\nu/R - \kappa RF) \\
q_2 &= 1 & q_0 &= -\kappa^2 + i\kappa/R & s_0 &= 1
\end{aligned}$$

Eq. (4.7) defines a generalized eigenvalue/eigenfunction problem. The eigenfunctions are the normal modes of the model, the real and the imaginary parts of each eigenvalue being the rate of growth and frequency of the associated mode.

For a given viscosity profile the parameter space of the problem contains *two* variables, the Reynolds number and the nondimensional wavenumber, which did not exist in the previous case. The effect of the bulk viscosity  $\nu(\infty)$  and angular velocity of the electrode  $\Omega$  appear in the definition of the Reynolds number.

Boundary conditions of the problem require non-slip flow and vanishing axial component of the velocity at the electrode surface. These conditions are already fulfilled by the base-state, so the hydrodynamic field cannot be modified by the perturbation at the electrode surface. In consequence we must require  $g = h = 0$  in  $\xi = 0$ . Moreover, we conclude from Eq. (4.4) that  $h' = 0$  at the electrode surface. In  $\xi \rightarrow \infty$  we require that the perturbation vanishes ( $g = h = 0$ ) and that  $h' = 0$ .

The generalized eigenvalue/eigenfunction problem is solved numerically. Space derivatives are represented by the following discrete formulæ transforming the original problem in an eigenvalue/eigenvector problem.

$$\begin{aligned} X'_i &= \frac{1}{2\Delta\xi}(-X_{i-1} + X_{i+1}) \\ X''_i &= \frac{1}{\Delta\xi^2}(X_{i-1} - 2X_i + X_{i+1}) \\ X'''_i &= \frac{1}{2\Delta\xi^3}(-X_{i-2} + 2X_{i-1} - 2X_{i+1} + X_{i+2}) \\ X''''_i &= \frac{1}{\Delta\xi^4}(X_{i-2} - 4X_{i-1} + 6X_i - 4X_{i+1} + X_{i+2}) \end{aligned}$$

The problem is solved using the LAPACK double precision *zgegv* routine for complex generalized nonsymmetric eigenproblems.

**4.1. Results.** In order to identify unstable regions the parameter space was spanned in the range  $10 \leq R \leq 600$  and  $0.05 \leq \kappa \leq 0.9$ . The constant viscosity case and four variable viscosity configurations were considered. In the cases of variable viscosity fluids we analysed three configurations with the viscosity at the electrode surface set to  $\nu(0)/\nu(\infty) = 6$  and  $q$  taking the values  $q = 15, 2$  and  $.05$  (see Eq. 2.13). The fourth variable viscosity case was run with  $\nu(0)/\nu(\infty) = 12$  and  $q = 2$ . It is worth to mention that the parameter  $q$  defines the slope of the viscosity profile close to the electrode surface and, consequently, the thickness of the viscosity boundary layer. In all simulations the system length was assumed as  $\xi_{max} = 20$  and the eigenvalue/eigenvector problem was solved in the nodes of a grid containing 400 uniformly spaced points. The results are presented in the form of a neutral stability diagram, shown in Fig. (5). The two hydrodynamic parameters of the problem, namely the Reynolds number and the non-dimensional wavenumber are represented in the  $x$  and  $y$  axes of this diagram, respectively. The neutral stability curves define the border between a stable and an unstable region. At low Reynolds numbers, all wavelengths are linearly stable. Upon increasing the Reynolds number a bifurcation point defined by the critical pair,  $(R_c, \kappa_c)$ , is eventually attained. Beyond the bifurcation point a range  $\kappa_{min} \leq \kappa \leq \kappa_{max}$ , of unstable modes exists.

The form of the diagram shown in Fig. (5) is typical of stability analysis of boundary layers velocity profiles with an inflection point that are, therefore, inviscidly unstable.

The critical Reynolds number for the constant viscosity case (curve 1) is found to be of the order of 215, corresponding to a critical wavenumber of the order of 0.32. These figures are within the range of critical parameters found in the literature for the stability analysis of constant viscosity boundary layers which develop close to rotating disks. For  $R = 500$  the range of unstable wavenumbers is approximately  $0.1 \leq \kappa \leq 0.55$ .

The introduction of a variable viscosity fluid drastically changes the stability properties of the

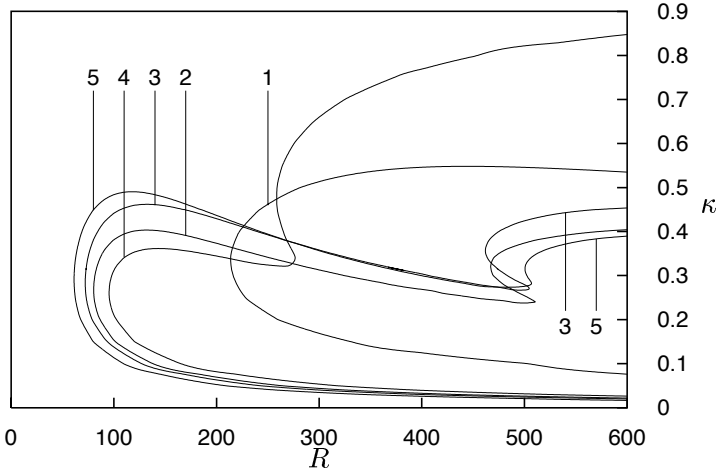


Fig. 5: Neutral stability curves for constant viscosity fluid (curve 1), variable viscosity fluids with  $\nu(0)/\nu(\infty) = 6$  and  $q$  taking the values  $q = 15, 2$  and  $.05$  (curves 2, 3, and 4). Curve 5 corresponds to a fluid with  $\nu(0)/\nu(\infty) = 12$  and  $q = 2$ .

boundary layer, in the sense of reducing the critical Reynolds number. Curve 2 was obtained by setting  $\nu(0)/\nu(\infty) = 6$  and  $q = 15$ . The critical Reynolds number decreases to less than 50% of the value corresponding to the constant viscosity case. In this case the viscosity boundary layer (the thickness across which the viscosity varies) is essentially confined to  $\xi < 1$ . For a comparison purpose we mention that the hydrodynamic boundary layer is confined to  $\xi < 8$ .

An increase in the thickness of the viscosity boundary layer, obtained by setting  $q = 2$  leads to a small reduction in the critical Reynolds number, as shown by curve 3. The viscosity boundary layer is essentially confined to  $\xi < 1$ , in this case. By keeping  $\nu(0)/\nu(\infty)$  constant and further increasing the thickness of the viscosity boundary layer, we obtain a too thick layer characterized by a high viscosity. Consequently, the unstabilization effect due to the variable viscosity of the fluid attains a limit and is eventually reversed if the thickness of the viscosity boundary layer is progressively increased. This effect is shown by curve 4, obtained with  $q = .05$ . In this case the viscosity boundary layer extends to  $\xi \approx 4$ .

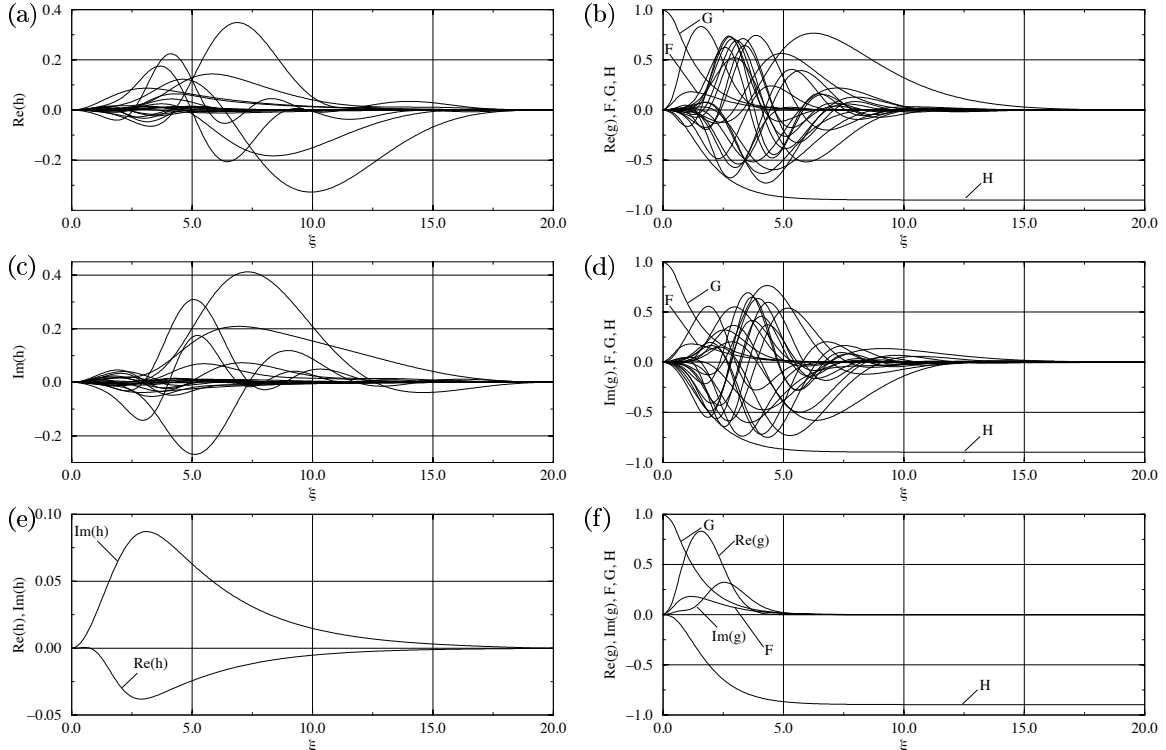


Fig. 6: (a):  $\Re(h)$ , (b):  $\Re(g)$ , (c):  $\Im(h)$ , (d):  $\Im(g)$ ; Real and Imaginary parts of first 20 less stable modes of perturbations with nondimensional wavelength  $\kappa = .30$ , obtained in  $R = 90$ . Fluid parameters are  $\nu(0)/\nu(\infty) = 6$  and  $q = 15$ . (e):  $\Re(h)$ ,  $\Im(h)$  and (f):  $\Re(g)$ ,  $\Im(g)$  real and Imaginary parts of the only unstable mode obtained with this parameter configuration.

Finally, an increase in the ratio  $\nu(0)/\nu(\infty)$  leads to a decrease in the critical Reynolds number, as shown by curve 5, Fig. (5).

Fig. (6) shows real and imaginary parts of the first 20 less stable modes of perturbations with nondimensional wavelength  $\kappa = .30$ , obtained in  $R = 90$ . Fluid parameters are  $\nu(0)/\nu(\infty) = 6$  and  $q = 15$ . This point is located in the unstable region of the diagram shown in Fig. (5), close to the bifurcation point of curve 2. Only one mode, shown in Fig. (6e) and (6f), is in fact unstable in this case.

**5. Conclusions.** In this work we studied how the linear stability of the hydrodynamic field developed close to a rotating disk electrode is affected by the introduction of a viscosity gradient along the rotating axis direction. Two classes of perturbations were considered: perturbations monotonically varying along the radial direction and perturbations periodically modulated along the radial direction.

By introducing the perturbed base state in the linearized evolution equations we arrived at a generalized eigenvalue/eigenfunction problem. Space derivatives were discretely represented, transforming the original problem in a generalized eigenvalue/eigenvector problem, which was numerically solved using standard routines for nonsymmetric eigenproblems.

The results show that the hydrodynamic field is always stable with respect to the first class of perturbations. It is worth to note that the stability problem associated to this class does not contain a Reynolds number, which is the bifurcation parameter defining the stability limit where a non-vanishing velocity field exists.

A totally different situation occurs when perturbations periodically modulated along the radial direction are considered. In this case, the stability is strongly affected by the gradient, and it can be said that the hydrodynamic field becomes *less* stable. Reductions of the order of 50% or even larger, on the critical Reynolds number, or the critical distance from the rotating axis, may be expected. This lower critical Reynolds number is of the order of magnitude of those attained in the experimental setup used by Ferreira (1993) and Geraldo (1998), supporting the idea that the current instabilities observed in the electrodissolution of iron rotating electrodes may be induced by a hydrodynamical instability.

The stability problem with respect to perturbations periodically modulated contains *four parameters*: the nondimensional radius or Reynolds number based on the angular velocity, the nondimensional perturbation wavelength,  $\nu(0)/\nu(\infty)$  and  $q$ , which defines the slope of the viscosity profile close to the electrode surface. The former two parameters depend on bulk characteristics of the system and on the length scale of the perturbation. The latter two are related to the electrodissolution kinetics and to the transport properties of the chemical species generated at the interface. It is worth to note that the above mentioned experimental data show that an increase in the fluid bulk viscosity, or a reduction in the electrode angular velocity stabilize the current oscillations. This result is captured by the stability analysis presented in this work, since both changes in the operational parameters lead to a decrease in the Reynolds number and to a more stable situation.

Part of the results presented in this work were already published in the proceedings of the 8<sup>th</sup> Brazilian Congress of Thermal Engineering and Sciences – ENCIT 2000.

**Acknowledgements** J. P. acknowledges financial support from CNPq (Brazil) through grant 452399/00-9 (NV). Numerical calculations were done at the High-Performance Computer Center (NACAD-UFRJ) and in the workstations of the Metallurgy and Materials Eng. Dept. (UFRJ). The authors acknowledge fruitfull discussions with prof. R. E. Kelly from the University of California at Los Angeles and R. M. Silva for the support in handling the workstations.

## REFERENCES

- [1] O. E. BARCIA, O. R. MATTOS, AND B. TRIBOLLET, *Anodic dissolution of iron in acid sulfate under mass transport control*, J. Electrochem. Soc., 139 (1992), pp. 446–453.
- [2] A. CAPRANI, C. DESLOIUS, S. ROBIN, AND B. TRIBOLLET, *Transient mass transfer at partially blocked electrodes*, J. Electroanal. Chem., 238 (1987), pp. 67–91.
- [3] T. CEBEKI AND K. STEWARTSON, *On stability and transition in three-dimensional flows*, AIAA J., 18-4 (1980), pp. 398–405.
- [4] T. C. CORKE AND K. F. KNASIAK, *Cross-flow instability with periodic distributed roughness*, in IUTAM Symposium on Nonlinear Instability and Transition in Three-Dimensional Boundary Layers, P. W. Duck and P. Hall, eds., Kluwer, 1996, pp. 267–282.
- [5] C. DESLOIUS, B. TRIBOLLET, DUPRAT, AND F. MORAN, *Transient mass transfer at a coated rotating disk electrode*, J. Electrochem. Soc., 134 (1987), pp. 2496–2501.
- [6] I. EPELBOIN, G. GABRIELLI, M. KEDDAM, J. C. LESTRACH, AND H. TAKENOUTI, *Passivation of iron in sulfuric acid medium*, J. Electrochem. Soc., 126 (1979), pp. 1632–1637.
- [7] J. R. R. M. FERREIRA, O. E. BARCIA, AND B. TRIBOLLET, *Iron dissolution under mass transport control: the effect of viscosity on the current oscillation*, Electrochim. Acta, 39 (1994), pp. 933–938.
- [8] A. B. GERALDO, O. E. BARCIA, O. R. MATTOS, F. HUET, AND B. TRIBOLLET, *New results concerning the oscillations observed for the system iron-sulfuric acid*, Electrochim. Acta, 44 (1998), pp. 455–465.

- [9] N. GREGORY, J. T. STUART, AND W. S. WALKER, *On the stability of three-dimensional boundary layers with application to the flow due to a rotating disk*, Phil. Trans. Roy. Soc. London, A-248 (1955), pp. 155–199.
- [10] R. KOBAYASHI, Y. KOHAMA, AND C. TAKAMADATE, *Spiral vortices in a boundary layer transition regime on a rotating disk*, Acta Mechanica, 35 (1980), pp. 71–82.
- [11] D. K. LILLY, *On the stability of ekman boundary flow*, J. Atm. Sci., 23 (1966), pp. 481–494.
- [12] M. R. MALIK, *The neutral curve for stationary disturbances in rotating-disk flow*, J. Fluid Mech., 164 (1986), pp. 275–287.
- [13] M. R. MALIK, WILKINSON, AND S. A. ORZAG, *Instability and transition in a rotating disk*, AIAA J., 19-9 (1981), pp. 1131–1138.
- [14] J. J. PODESTA, R. C. V. PIATTI, AND A. J. ARVIA, *The potentiostatic current oscillations at iron/sulfuric acid solution interfaces*, J. Eletrochem. Soc., 126 (1979), pp. 1363–1367.
- [15] R. POLLARD AND J. NEWMAN, *Silicon deposition on a rotating disk*, J. Eletrochem. Soc., 127 (1980), pp. 744–752.
- [16] J. PONTES, N. MANGIAVACCHI, O. E. BARCIA, O. R. MATTOS, B. TRIBOLLET, AND D. WALGRAEF, *Stability of the hydrodynamic field close to a rotating disk electrode*, in Proceedings of the 8<sup>th</sup> Brazilian Congress of Thermal Engineering and Sciences, Brazil, 2000. paper S35P31 (in CD).
- [17] H. L. REED AND W. S. SARIC, *Stability of three-dimensional boundary layers*, Ann. Rev. Fluid Mech., 21 (1989), pp. 235–84.
- [18] P. RUSSEL AND J. NEWMAN, *Current oscillations observed within the limiting current plateau for iron in sulfuric acid*, J. Eletrochem. Soc., 133 (1986), pp. 2093–2097.
- [19] H. SCHLICHTING, *Boundary Layer Theory*, McGraw-Hill, 1968.
- [20] N. SMITH, *Exploratory investigation of laminar boundary layer oscillations on a rotating disk*, Tech. Rep. TN-1227, NACA, Dec. 1946.
- [21] K. STEWARTSON AND C. J. SIMPSON, *The unsteady boundary layer on a rotating disk in a counter rotating fluid. Part 2*, J. Fluid Mech., 121 (1982), pp. 507–515.
- [22] B. TRIBOLLET AND J. NEWMAN, *The modulated flow at a rotating disk electrode*, J. Eletrochem. Soc., 130 (1983), pp. 2016–2026.
- [23] T. VON KÁRMÁN AND Z. ANGEW, *Über laminare und turbulente reibung*, Math. Mec., 1 (1921), pp. 233–252.
- [24] S. WILKINSON AND M. M. R., *Stability experiments in the flow over a rotating disk*, AIAA J., 23 (1985), p. 588.